Transitions from spatiotemporal chaos to cluster and complete synchronization states in a shift-invariant set of coupled nonlinear oscillators

Y. Chembo Kouomou[1,2] and P. Woafo[1,*]

[1]*Laboratoire de Mécanique, Faculté des Sciences, Université de Yaoundé I, Boîte Postale 812 Yaoundé, Cameroon*
[2]*Division of Telecommunication Technical Studies, Minpostel, Yaoundé, Cameroon*
(Received 18 July 2002; revised manuscript received 2 December 2002; published 11 April 2003)

We study the spatiotemporal dynamics of a ring of diffusely coupled single-well Duffing oscillators. The transitions from spatiotemporal chaos to cluster and complete synchronization states are particularly investigated, as well as the Hopf bifurcations to instability. It is found that the underlying mechanism of these transitions relies on the motion of the representative points corresponding to the system's nondegenerated spatial transverse Fourier modes in the parametric Strutt diagram. A scaling law is used to demonstrate that the compact interval of the scalar coupling parameter values leading to cluster synchronization broadens in a square-power-like fashion as the number of oscillators is increased. The analytical approach is confirmed by numerical simulations.

I. INTRODUCTION

The study of the (non) synchronous behavior of coupled chaotic oscillators is currently gathering a growing amount of important experimental and theoretical contributions [1–7]. The interest devoted to that topic is motivated by its potential relevance to pattern formation and coherent collective behavior in physics (Josephson junctions, granular hydrodynamics), chemistry (discrete reaction-diffusion systems), and biology (development of living organisms, collective dynamics of biological cells aggregates).

Beside the well known and intensively studied phenomena of spatiotemporal chaos [8] and complete (full) synchronization [9] in coupled chaotic systems, recent literature has reported the existence of hybrid configurations consequent to symmetry breaking and spontaneous spatial reordering, which are sometimes referred to as cluster synchronization [4–6]. These intermediary states allow the chaotic oscillators to synchronize with one another in groups, while there is no synchronization among the groups. Clustering is mostly witnessed when the coupling is nonlocal or nonsymmetric [5,10]. It consequently appears as more fascinating and more unconventional when it occurs in a system with local and symmetric coupling [4,6].

Depending on the number of chaotic oscillators, the type of coupling, and the boundary conditions, the dynamical system can display a rich but limited set of different cluster patterns. The stability of the various clusters is usually studied through the variations of the sub-Lyapunov exponents associated with their related submanifolds. Unfortunately, this numerical procedure is very time consuming and, moreover, very repetitive, since the numerical simulation of the sub-Lyapunov exponents has to be performed separately for each possible cluster. Therefore, this approach can no longer be applied when the number of oscillators becomes prohibitively high.

In this paper we consider a ring of N diffusely coupled single-well Duffing oscillators and we aim to give an analytic insight into the various transitions that can occur between the three possible dynamical states of the ring (spatiotemporal chaos, cluster synchronization, complete synchronization) and instability when the coupling strength is varied. However, our analytical study presents, within the same framework, the underlying structure of both the states themselves and the transitions between them. This may have valuable applications in the thermodynamic limit ($N \rightarrow +\infty$) for the phase transitions theory of one-dimensional atomic lattices, or for nonlinear transmission lines in communication engineering.

The paper is organized as follows. In Sec. II we perform the general stability analysis of the model, and we use Floquet theory to derive approximated analytical stability boundaries for the spatial Fourier modes of the ring. The Hopf bifurcations between the various dynamical states of the model will be particularly analyzed. Section III deals with the extension of the study to the thermodynamic limit, and with the application of the stability analysis to the specific cases of a positive and of a negative nonlinear stiffness coefficient. A scaling law is used to demonstrate that the transition boundaries of any N-ring can be recurrently deduced from the transition boundaries of the corresponding two-oscillators model. Finally, Sec. IV is devoted to the Conclusion.

II. THEORETICAL STABILITY ANALYSIS, CRITICAL TRANSITION BOUNDARIES, AND NUMBERING OF CLUSTERS

A. The stability analysis

The coupled system under study is a ring of N diffusely coupled single-well Duffing oscillators (SWDOs) whose evolution equations are

$$\ddot{x}_i + \lambda \dot{x}_i + x_i + \gamma x_i^3 = F \cos \omega t + K(x_{i+1} - 2x_i + x_{i-1}),$$

$$i = 1,...,N. \tag{1}$$

_____
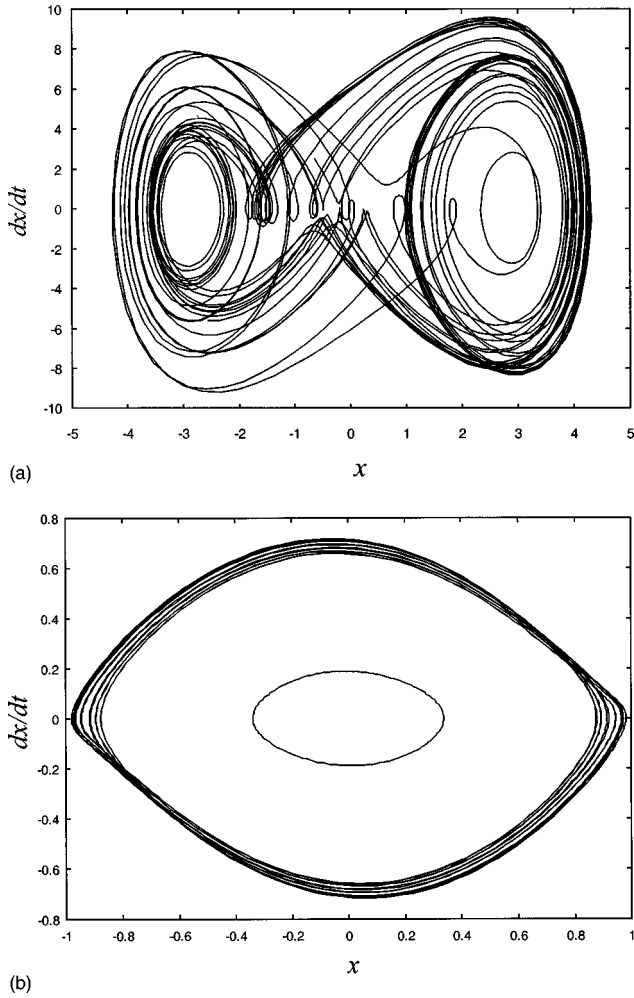*Corresponding author. Email address: pwoafo@uycdc.uninet.cm

(a)

(b)

FIG. 1. Phase plane for the chaotic oscillators (a) $\gamma > 0$ case: $\lambda = 0.2$; $\gamma = 1.0$; $F = 28.5$; $\omega = 0.86$, with initial conditions (0,0). (b) $\gamma < 0$ case: $\lambda = 0.4$; $\gamma = -1.0$; $F = 0.23$; $\omega = 0.5255$, with initial conditions $(-0.3, 0.7)$ for the chaotic trajectory, and (0, 0) for the regular inner limit cycle. The $\gamma > 0$ and $\gamma < 0$ cases will always refer to these parameters throughout the whole paper.

$x_i(t)$ is the instantaneous deviation of the ith oscillator from the stable and trivial equilibrium state $x_i \equiv 0$. λ stands for the damping, and γ is a nonlinear stiffness coefficient which may be either positive or negative. Each oscillator of the ring is excited by a periodic excitation of amplitude F and frequency ω. At last, the positive parameter K is the scalar coupling strength. The system of Eqs. (1) obeys the shift-invariance condition $x_{i+N} \equiv x_i$. When $K = 0$, each SWDO is uncoupled and displays a rich variety of nonlinear behaviors, depending on the chosen sets of parameters [11]. Figure 1 presents the typical chaotic oscillations that can be observed in SWDOs for both the $\gamma > 0$ and $\gamma < 0$ cases. As one can notice in Fig. 1(b), the $\gamma < 0$ oscillator is a bistable system, since the nonlinear oscillations may be either chaotic (outer attractor) or periodic (inner regular limit cycle), depending on the initial conditions.

The stability of the coupled system can be studied through the linearization of Eqs. (1) around the states x_i, according to

$$\ddot{\xi}_i + \lambda \dot{\xi}_i + (1 + 3\gamma x_i^2)\xi_i = K(\xi_{i+1} - 2\xi_i + \xi_{i-1}), \quad i = 1,\dots,N, \tag{2}$$

where ξ_i is the first order perturbation of x_i. We can replace in the first approximation the N distinct x_i chaotic variables of the parametric excitation by a unique variable x_0 which represents the dynamics of an uncoupled oscillator. This substitution enables us to uncouple the variational Eqs. (2) through a Fourier transform diagonalization [9], so that they can be rewritten as

$$\ddot{\zeta}_s + \lambda \dot{\zeta}_s + \left[1 + 3\gamma x_0^2 + 4K \sin^2\left(\frac{\pi s}{N}\right) \right]\zeta_s = 0, \quad s = 0,\dots,N-1, \tag{3}$$

where the ζ_s are new variational variables expressed in the diagonal base. The mode $s = 0$ is called the longitudinal mode because it governs the dynamics of the perturbations within the synchronization manifold, while the modes $s \neq 0$ are the transverse modes since they decide the linear stability of the perturbations transverse to the synchronization manifold.

The best deterministic candidates to replace the chaotic variable x_0 in the parametric term of Eq. (3) are the unstable periodic orbits (UPOs) of the chaotic attractor. They are in general multiperiodic, so that straightforwardly using them for the stability analysis would imply the resolution of an ordinary differential equation (ODE) with multifrequency parametric excitations. Hence, analytic stability boundaries may hardly be derived in that case. In fact, previous studies have shown that such a complexity can be avoided when the fundamental Fourier component is strong relatively to the harmonics of the external forcing frequency. It has been demonstrated in [12] for Van der Pol oscillators, in [13] for SWDOs, and in [14] for Rössler oscillators that for such chaotic oscillators, a single period-one approximation of the UPOs is sufficient to describe accurately the stability pattern of the coupled system. Figure 2 displays the Fourier spectra of the uncoupled SWDOs in both the $\gamma > 0$ and $\gamma < 0$ cases, and it clearly appears that the fundamental spectral component is predominant relative to the others, and is more likely to provoke the parametric resonance leading to desynchronization or instability. A sharper analysis would have also demonstrated that the parametric resonances induced by the harmonics of ω are easily stabilized by the nonlinear variational terms we have neglected in Eq. (2). Obviously, it results from Fig. 2 that the validity of the single-frequency approximation is more justified for the $\gamma < 0$ case than for the $\gamma > 0$ case.

Therefore, we approximate the chaotic variable x_0 with the uniperiodic function x_{per} defined as

$$x_{per}(t) = A_0 \cos(\omega t - \varphi). \tag{4}$$

The analytic amplitude A_0 can be determined through the Ritz variational criterion as 3.323 for the $\gamma > 0$ case. For the $\gamma < 0$ case, we rather have $A_0 = 0.343$ for the inner limit cycle and $A_0 = 0.864$ for the chaotic trajectory.

(a)

(b)
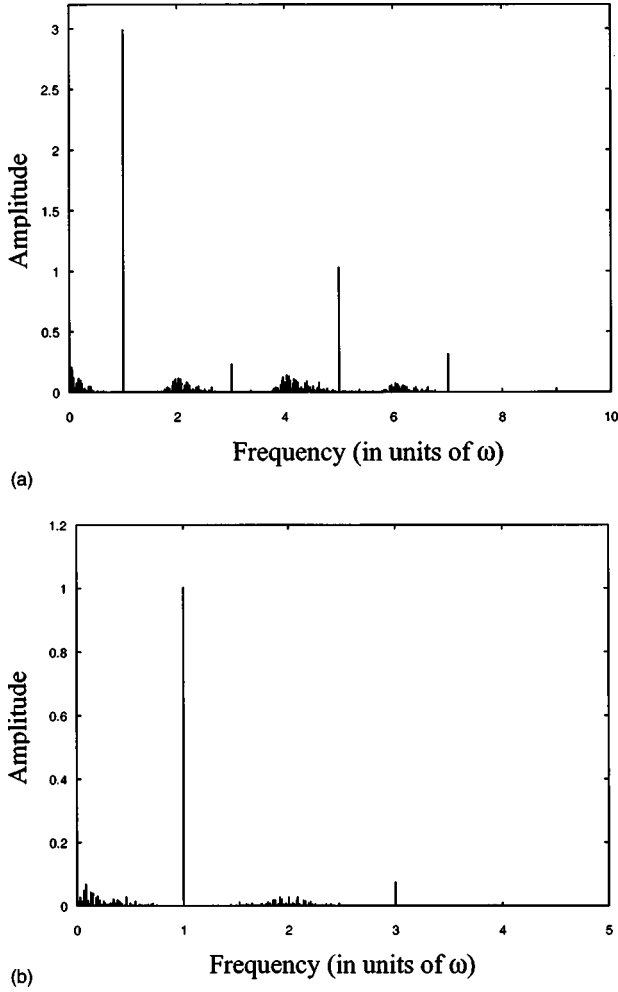
FIG. 2. Fourier spectra (a) $\gamma > 0$ case and (b) $\gamma < 0$ case.

The meaning of Eq. (4) is not to suppose initially a synchronous motion in the ring, even though it may seem to be its most obvious consequence: the essence of the substitution (4) is spectral and not dynamical, and hence, we implicitly assume that the spectral properties of the oscillators are not drastically modified by the coupling. In that case, the variational equations (3) can be rewritten in their turn under the form of canonical Mathieu equations

$$\frac{d^2 \eta_s}{d\tau^2} + [\delta_s + 2\alpha \cos(2\tau - 2\varphi)]\eta_s = 0, \quad s = 0,...,N-1 \tag{5}$$

with the following rescalings:

$$\tau = \omega t,$$

$$\eta_s(\tau) = \zeta_s \exp\left(\frac{\lambda \tau}{2\omega}\right),$$

$$\delta_s = \frac{1}{\omega^2}\left[1 + \frac{3}{2}\gamma A_0^2 - \frac{\lambda^2}{4} + 4K \sin^2\left(\frac{\pi s}{N}\right)\right], \tag{6}$$
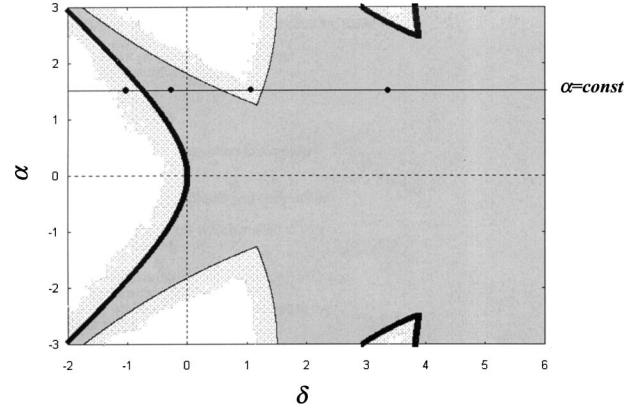

FIG. 3. The Strutt diagram. The linearly stable area is darkly shaded, the nonlinearly stable belt is lightly shaded, and the unstable area is blank. The π periodic boundaries are denoted by thick lines while the 2π periodic boundaries are denoted by thin lines. The representative points of four nondegenerated modes have also been represented.

$$\alpha = \frac{3\gamma A_0^2}{4\omega^2}.$$

One should notice that the feedback parameter K and the number of oscillators N only influence δ_s and not α anyway. From Floquet theory, it can therefore be demonstrated that a given mode s is linearly stable if the following double inequality is fulfilled [13,15]:

$$-\sinh^2\left(\frac{\lambda \pi}{4\omega}\right) < \Gamma(\delta_s, \alpha) < +\cosh^2\left(\frac{\lambda \pi}{4\omega}\right), \tag{7}$$

where

$$\Gamma(\delta, \alpha) = \begin{cases} \Delta(\delta, \alpha)\sin^2\left(\frac{1}{2}\pi\sqrt{\delta}\right) & \text{if } \delta \geq 0 \\[2mm] -\Delta(\delta, \alpha)\sinh^2\left(\frac{1}{2}\pi\sqrt{-\delta}\right) & \text{if } \delta < 0 \end{cases} \tag{8a}$$

and

$$\Delta(\delta, \alpha) = \left\| \delta_{m,n} + \frac{\alpha(e^{2i\varphi}\delta_{m,n-1} + e^{-2i\varphi}\delta_{m,n+1})}{\delta - (2m)^2} \right\|. \tag{8b}$$

$\Delta(\delta, \alpha)$ is the infinite Hill determinant evaluated on a periodic boundary of η. The $\delta_{m,n}$ are the Kronecker symbols, m and n being integers varying from $-\infty$ to $+\infty$.

From a conventional approach, the parametric plane (δ, α) is divided into two areas: the area of linear stability ($\zeta_s \to 0$) and the area of linear instability ($\zeta_s \to \pm\infty$). The boundaries between these two zones can be either π periodic [i.e., $\zeta(t) = \zeta(t + \pi/\omega)$] if $\Gamma(\delta, \alpha) = -\sinh^2(\lambda\pi/4\omega)$ or 2π periodic [i.e., $\zeta(t) = \zeta(t + 2\pi/\omega)$] if $\Gamma(\delta, \alpha) = +\cosh^2(\lambda\pi/4\omega)$. The corresponding stability diagram is sometimes referred to as the Strutt diagram and is represented in Fig. 3. The linearly stable area is enclosed within

the π and 2π periodic boundaries, and has been uniformly shaded. It is known that crossing these periodic boundaries corresponds to Hopf bifurcations [13,15]. In Fig. 3 four non-degenerated modes have been represented on a $\alpha = \text{const}$ straight horizontal line. The leftmost point represents the longitudinal mode, while the remaining three others are transverse modes.

B. Transition boundaries between the cluster states

In fact, the Strutt diagram may be divided into two only at the linear approximation. When the variational equations aim to decide the stability of a nonlinear system, the nonlinear terms that have been discarded in the variational equations (2) play a predominant stabilizing role, thereby leading to the emergence of a third area in the Strutt diagram. Effectively, due to these nonlinear variational terms, there is a buffer zone between the linearly stable and linearly unstable areas: it is an area of nonlinear stability (which is, however, linearly unstable), where $|\zeta_s|$ does not decay to zero and does not grow to infinity either. The inner boundaries of this buffer zone are the periodic boundaries of the linearly stable area, while its outer boundaries with the unstable area are very irregular and sometimes fractal-like. In Fig. 3 this area of nonlinear stability has been represented as a lightly shaded belt surrounding the linearly stable area, while the unstable one remains blank. Among the four modes represented, the first and third modes (starting from the left) are nonlinearly stable while the two others are linearly stable. Let us assume that the local width of this belt is $\Lambda(\delta^{(k\pi)}, \alpha)$, where the couple $(\delta^{(k\pi)}, \alpha)$ is the related point situated on a $k\pi$ periodic boundary of the Strutt diagram ($k = 1$ or 2). Assuming that the transverse modes are in the right-half plane, the analytical condition of nonlinear stability can be approximated for each of them by

$$(-1)^k (\delta_s - \delta^{(k\pi)}) \left[\sin^2\left(\frac{1}{2}\pi\sqrt{\delta^{(k\pi)}}\right) \frac{\partial \Delta(\delta_s, \alpha)}{\partial \delta_s}\bigg|_{\delta_s = \delta^{(k\pi)}} \right.$$
$$\left. + \frac{\pi}{4} \frac{\sin(\pi\sqrt{\delta^{(k\pi)}})}{\sqrt{\delta^{(k\pi)}}} \Delta(\delta^{(k\pi)}, \alpha) \right]$$
$$< \frac{\Lambda(\delta^{(k\pi)}, \alpha)\cosh\left(\dfrac{\lambda\pi}{2\omega}\right)}{|\delta^{(\pi)} - \delta^{(2\pi)}|}. \qquad (9)$$

Here $(\delta^{(k\pi)}, \alpha)$ is the nearest boundary point relative to the representative point $M_s(\delta_s, \alpha)$, while $|\delta^{(\pi)} - \delta^{(2\pi)}|$ in the rhs of Eq. (9) is the length of the segment laying within the nearest stability interval. For the geometrical reasoning, the local belt width $\Lambda(\delta^{(k\pi)}, \alpha)$ can be replaced without any inconvenience by its average value $\overline{\Lambda}$.

We can now analyze through the Strutt diagram what is happening in the coupled system when the coupling strength K is increased. When $K = 0$, the system is uncoupled and all the transverse modes $s \neq 0$ degenerate into the longitudinal mode $s = 0$. Therefore, the whole coupled system is represented by a single point M_0 of coordinates (δ_0, α) in the

Strutt diagram. Since the uncoupled system is chaotic, it clearly appears that the point M_0 is situated within the nonlinear stability area. As K is increased, the $N - 1$ transverse modes represented in the Strutt diagram by the points $M_s(\delta_s, \alpha)$ independently begin to move along the straight horizontal line of equation $\alpha = \text{const}$ with a ''velocity''

$$\nu_s = \frac{d\delta_s}{dK} = \frac{4}{\omega^2} \sin^2\left(\frac{\pi s}{N}\right), \quad s = 1, \ldots, N - 1. \qquad (10)$$

Hence, depending on K and N, the points M_s are distributed between the different areas of the Strutt diagram, i.e., each transverse mode may be either linearly stable, nonlinearly stable, or unstable.

Therefore, depending on K and N, three distinct sets of mode distributions, which are unambiguously equivalent to the three dynamical states of the ring, can be distinguished. In the first case, all the transverse modes are within the area of nonlinear stability: it corresponds to the regime of spatiotemporal chaos. For the second case, certain transverse modes are in the area of linear stability while all the others are in the zone of nonlinear stability: it is the regime of cluster synchronization. For the third case, all the transverse modes are linearly stable, and then, the ring is in the complete synchronization state. Hence, the mode distribution of Fig. 3, for example, corresponds to a cluster synchronization state. At last, when at least one transverse mode is in the instability area, the whole coupled system becomes unstable, i.e., the state variables x_i indefinitely grow to infinity. The principal advantage of reasoning through the Strutt diagram is that increasing the number of oscillators does not require us to sketch different stability maps, but just to conveniently add supplementary transverse modes on the same diagram.

We emphasize one more time that the validity of our modal approach for the study of the ring's dynamical behavior strongly depends on the nature of the Fourier spectra of the individual uncoupled oscillators. It is only because the fundamental Fourier component is overly strong relatively to all the others that we can, for example, interpret in first approximation the spatiotemporal chaos state as the result of linearly unstable spatial Fourier modes. In the general case, it is known that this interpretation is absolutely not valid.

C. Numbering of clusters

It appears from the above analysis that cluster synchronization is the result of the distribution of the transverse modes between the linear and nonlinear stability areas of the Strutt diagram. From the discrete eigenfrequency spectrum of Eq. (3), one can deduce that the number of nondegenerated transverse modes is $N/2$ if N is even and $(N-1)/2$ if N is odd. Hence, distributing $N/2$ [or $(N-1)/2$] points amongst two areas yields $2^{N/2}$ (or $2^{(N-1)/2}$) different possibilities. Provided that spatiotemporal chaos (all the transverse modes are nonlinearly stable) and complete synchronization (they are all linearly stable) are excluded, the number of possible cluster states can be deduced as

$$\aleph = \begin{cases} 2^{N/2} - 2 & \text{if } N \text{ is even} \\ 2^{(N-1)/2} - 2 & \text{if } N \text{ is odd,} \end{cases} \quad \text{where } N \geqslant 2. \quad (11)$$

It is, however, important to notice that mathematically, spatiotemporal chaos and cluster synchronization correspond to an N cluster and to a one cluster, respectively. For small values of N, the following results are obtained. When $N=2$ or $N=3$, linearly stable clustering is not observed: we notice either spatiotemporal chaos (*ab* and *abc* states) or a completely synchronous motion (*aa* and *aaa*). For $N=4$, two cluster states are foreseen by Eq. (11); anyway, symmetry considerations allow the *abab* state to exist, while the state *aabb* is unstable and is not observed [16]. The same reasoning applies for $N=5$ as well. The case $N=6$ has been intensively studied by Zhang and co-workers in [4] for Rössler oscillators. Five different cluster patterns have been observed (while $\aleph=6$), since the sixth state *aaabbb* is always unstable. Note that the mode distribution of Fig. 3 can correspond to a ring of 6 or 7 oscillators.

When N is further increased, the number of possible clusters grows exponentially according to Eq. (11). Anyway, it should be stressed that some of these clusters are scarcely or not observed during numerical simulations or in practice. Three main reasons can explain that. The first reason is that some clusters are very weakly stable, so that they rapidly degenerate into compatible clusters of higher symmetry (i.e., less complicated and more stable patterns). This explains why for a given K, it is sometimes possible to obtain many different clusters, depending on the initial conditions [4]. The second reason is that for a fixed number of oscillators N, it may be impossible to witness a given cluster state because the transverse modes do never fit with the related mode distribution in the Strutt diagram, whatever the value of K is. The third and last reason is that when the cluster state corresponds to a situation where only very few nondegenerated modes are linearly stable, a global correlation between the ring variables is witnessed, rather than localized mutual synchronization states. In that case, the ring is said to be in the "rotating wave state." Here and throughout the whole paper, we refer to any spatial ordering, either by effective synchronization of some items of the ring or by a global correlation between the state variables, as cluster synchronization, since the above analysis shows that both the "hard" cluster synchronization (almost all the transverse modes are linearly stable) and the "rotating wave state" (only a few of them are linearly stable) have exactly the same mathematical nature, even though the related dynamical consequences are different. From our Strutt diagram approach, the emergence from spatiotemporal chaos occurs when the fastest Fourier mode becomes linearly stable while all the others remain nonlinearly stable. Hence, one can conclude that emergence from spatiotemporal chaos first passes through an "ordering," i.e., a bifurcation to a "rotating wave state."

Another marginal phenomenon can be reported. The numbering of the cluster states in Eq. (11) relies on the fact that the eigenfrequency spectrum is approximately half-degenerated, since the number of figurative transverse mode points in the Strutt diagram is $N/2$ or $(N-1)/2$. In reality, it

may be possible in some particular cases that the nonlinear variational terms we have discarded in Eq. (3) succeed in destroying the partial degeneracy of the linear Fourier eigenfrequency spectrum, thereby inducing a number of figurative points higher than $N/2$ or $(N-1)/2$. Therefore, the exponent of 2 in Eq. (11) increases so that new "unconventional" cluster states do emerge, such as *abcb*, for example, when $N=4$. This phenomenon can be identified to a kind of nonlinear mode-locking.

Consequently, since Eq. (11) does not take into account these considerations, $\aleph$ can just be considered as an order of magnitude. However, one can expect that this quantitative estimation may be useful for the statistical approach of the model in the thermodynamic limit.

III. NUMERICAL SIMULATIONS

We focus in this section on some of the corollaries of the above theoretical stability analysis for the specific cases of a positive and of a negative nonlinear stiffness coefficient, respectively. As we have earlier noticed, the number of clusters is low when rings of only few oscillators are concerned. For these cases, numerical simulation can be performed to study each cluster state as well as the transitions amongst them. However, this approach does not hold anymore when N is significantly increased, since it becomes quite complicated to identify the various clusters. Moreover, these clusters become less interesting as individuals when N is high.

The appropriate approach in this case is to identify in the parametric plane N-K the areas corresponding to each of the three dynamical states of the ring. A scaling law is generally used for that purpose [1,2], and we hereafter proceed in that way to derive the stability pattern of the N-oscillator system from the stability pattern of the two-oscillators model. The potential interest of such a scaling law is high in the thermodynamic limit: it means that the dynamical states and the phase transitions of a one-dimensional lattice model can be deduced from the experimental or theoretical data obtained through the study of the two-oscillators model interactions.

1. The $\gamma > 0$ case

Let us first consider the $\gamma > 0$ case. For $N=2$, numerical simulations show that the coupled system is nonsynchronized when $K \leqslant K_{b1}(2) = 0.34$, and synchronized for $K \geqslant K_{b2}(2) = 1.15$. For $K_{b1}(2) < K < K_{b2}(2)$, intervals of synchronized and nonsynchronized behavior are intermingled. This may easily be understood from the Strutt diagram interpretation. For a two-oscillator system, there is a single transverse mode moving along the $\alpha = \text{const}$ straight horizontal line. Its representative point M_1 starts from a nonlinear stability area, and then alternatively passes through linear and nonlinear stability zones. Finally, this point remains in the last semi-infinite segment laying within the linear stability region, leading to synchronous motion [13].

For $N>2$, the number of transverse modes becomes greater and the fastest of them has a velocity

$$\nu_{\text{fast}} = \begin{cases} \dfrac{4}{\omega^2} & \text{if } N \text{ is even} \\[2mm] \dfrac{4}{\omega^2} \sin^2\!\left(\dfrac{N-1}{2N}\pi\right) & \text{if } N \text{ is odd} \end{cases} \qquad (12a)$$

while the slowest has a velocity

$$\nu_{\text{slow}} = \frac{4}{\omega^2} \sin^2\!\left(\frac{\pi}{N}\right). \qquad (12b)$$

We can deduce from the stability analysis that when K is (very) low, all the transverse modes points M_s are spread within the initial nonlinear stability area, and therefore the ring displays a spatiotemporal chaotic dynamics. As soon as the fastest transverse mode point M_{fast} oversteps its first Hopf periodic boundary, the ring enters into the clustering regime and when the slowest mode M_{slow} oversteps its last Hopf periodic boundary, the coupled system becomes completely synchronized. The consequence of this transition mechanism is that it is impossible for the ring to become unstable, whatever the values of K and N are. In fact, this may be explained by a high $\bar{\Lambda}$ value.

Mathematically, if we define

$$K_{b1}(N) = \begin{cases} K_{b1}(2) & \text{if } N \text{ is even} \\[2mm] \dfrac{K_{b1}(2)}{\sin^2\!\left(\dfrac{N-1}{2N}\pi\right)} & \text{if } N \text{ is odd} \end{cases} \qquad (13)$$

and

$$K_{b2}(N) = \frac{K_{b2}(2)}{\sin^2\!\left(\dfrac{\pi}{N}\right)} \cong \frac{K_{b2}(2)}{\pi^2}N^2 \quad \text{when } N \gg 2. \quad (14)$$

It appears that the system is in the spatiotemporal regime if $K \le K_{b1}(N)$, in the completely synchronous state if $K \ge K_{b2}(N)$, and in the clustering regime when $K_{b1}(N) < K < K_{b2}(N)$. Hence, according to the scaling laws (13) and (14), the width $[K_{b2}(N) - K_{b1}(N)]$ of the clustering interval broadens in a square power-like fashion as N tends to infinity. The parametric plane N-K is therefore divided into three areas, as displayed in the semilogarithmic diagram of Fig. 4(a). Typically, we have spatiotemporal chaos for low K, cluster synchronization for intermediate values, and finally complete synchronization when K is high enough. One should anyway note that degenerated full synchronization states can also be observed in the cluster area, depending on the initial conditions and on the number of oscillators.

The numerical simulations confirm the above analysis. If, for example, we focus on the transition from the cluster to the completely synchronous states, we can notice the excellent coincidence between the numerical and the semi-analytical curves in Fig. 4(a). This good concordance is due to the fact that $K_{b2}(2)$ has been determined numerically (which is why we refer to this comparison as a semi-analytical one). A purely analytical comparison would re-
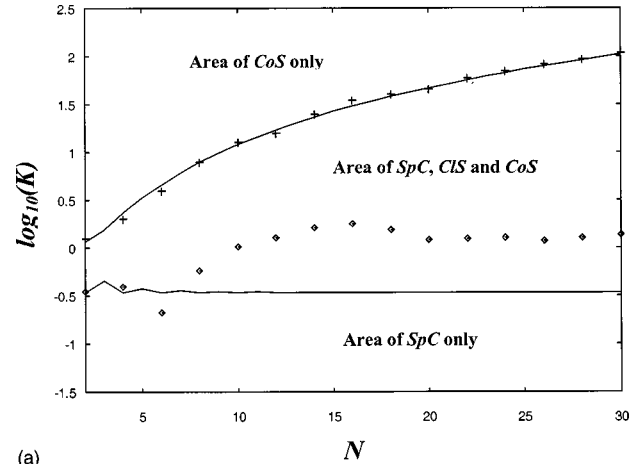
(a)
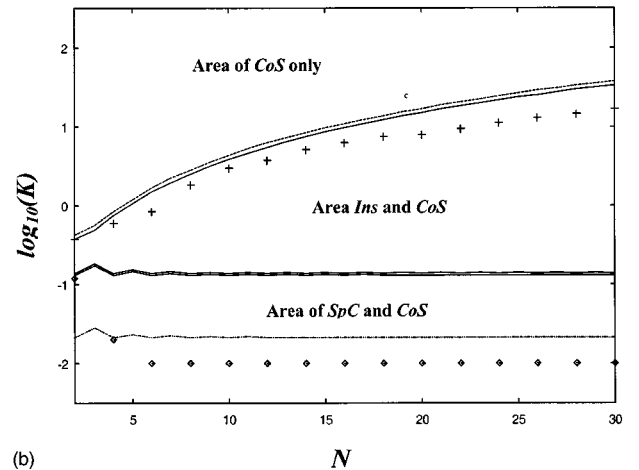
(b)

FIG. 4. Boundaries delimiting the different dynamical states and instability of the ring in the semilogarithmic diagram $N - \log_{10}(K)$. The analytical and semianalytical results are denoted by solid lines, while the numerical results are denoted by squares and crosses. "SpC" stands for spatiotemporal chaos, "CoS" for complete synchronization, "ClS" for cluster synchronization, and "Ins" for instability. Note that for the numerical comparisons, the drifts and deviations are accentuated by the logarithmic scale. (a) $\gamma > 0$ case. (b) $\gamma < 0$ case.

quire the analytic determination of $K_{b2}(2)$. This is difficult to achieve here because A_0 and the corresponding α constant value are so high that approximated or perturbation methods do not apply. Hence, for an analytic derivation of $K_{b2}(2)$, it would be indispensable to compute the Hill determinant $\Delta(\delta, \alpha)$ at a high order of truncation (≥ 18), or alternatively to use the Mathieu special functions. However, the purely analytic comparison would have presented a little discrepancy with the numerical results because Eq. (4a) does not qualitatively fit with the pseudo-double-well configuration of the phase portrait of Fig. 1(a).

If we now focus on the transition from spatiotemporal chaos to cluster synchronization, we can notice on Fig. 4(a) the rather good qualitative concordance between semi-analytical and numerical results. In fact, since Eq. (4) does not dynamically take into account the complex spatial patterns of spatiotemporal chaos and cluster synchronization

states, the bifurcation boundary $K_{b1}(N)$ is not as accurate as $K_{b2}(N)$, even though $K_{b1}(2)$ is also determined numerically. Nevertheless, its interest remains at least qualitative, however, since it predicts that the bifurcation values leading to the emergence of ordering from spatiotemporal chaos are roughly independent of N. It is also important to notice that the good concordance of our semianalytical comparison proves that as we have earlier postulated, the spectral properties of the coupled oscillators do not drastically differ from those of the corresponding uncoupled items.

2. The $\gamma < 0$ case

For the $\gamma < 0$ case, numerical simulations also confirm the theoretical analysis. When $N = 2$, one can numerically observe a synchronous motion when $K \leq K_{b1}(2) \approx 0.13$, and when $K \geq K_{b2}(2) \approx 0.37$. The crucial parameters $K_{b1}(2)$ and $K_{b2}(2)$ can here be determined analytically, thereby permitting a purely analytical comparison beside a semianalytical one. Effectively, the A_0 values in the $\gamma < 0$ case are low enough to enable an approximated analytical determination of both $K_{b1}(2)$ and $K_{b2}(2)$. At the first order approximation, the two branches of the 2π periodic boundaries around $\delta = 1$ can be derived as

$$\delta = 1 \pm \alpha \qquad (15)$$

so that for the outer chaotic trajectory ($A_0 = 0.864$), the bifurcation boundary values for $N = 2$ are

$$K_{b1}(2) = \frac{1}{16}(\lambda^2 - 3\gamma A_0^2) = 0.138,$$

$$K_{b2}(2) = \frac{1}{16}(\lambda^2 - 9\gamma A_0^2) = 0.416, \qquad (16)$$

which are in excellent concordance with the numerical values 0.13 and 0.37.

For the intermediate coupling strengths values [i.e., between $K_{b1}(2)$ and $K_{b2}(2)$], intervals of instability and of complete synchronization are intermingled. Here, the transitions cannot be well determined because they depend on the initial conditions [13]. Effectively, the multistability is so predominant in the $\gamma < 0$ case that stable motion is witnessed only when the initial conditions of all the oscillators are gathered within a small region of the ring phase space. From a Strutt diagram interpretation, we can say that the average width $\bar{\Lambda}$ is so thin that the nonlinear stability buffer zone is almost exclusively fractal-like. Therefore, one can straightforwardly deduce that clustering is practically impossible in the $\gamma < 0$ case for the chosen parameters, as well as spatiotemporal chaos independently of K and N. Consequently, the coupled system is generally either unstable or completely synchronous, except for very low K values, for which spatiotemporal chaos can be observed. Anyway, the fastest and the slowest transverse modes are expressed as for the $\gamma > 0$ case, so that the same scaling law reasoning applies. Hence, if we define $K_{b1}(N)$ and $K_{b2}(N)$ as in Eqs. (13) and (14), respectively, we can also divide the N-K plane into an upper zone of synchronous motion, an intermediate zone of inex-

tricably intermingled stable and unstable areas, and a lower zone of complete synchronization and spatiotemporal chaos. Naturally, the uncertainty on $K_{b1}(2)$ and $K_{b2}(2)$ induces an error when evaluating $K_{b1}(N)$ and $K_{b2}(N)$, but the square-power broadening behavior is preserved, however, and the scaling law remains at least of qualitative interest.

In Fig. 4(b) the uppermost double line stands for both the analytical and semianalytical results, and they indicate the bifurcation boundary to the completely synchronous state. These two solid lines are very near each other because of the excellent concordance between the numerical and analytical values of $K_{b2}(2)$ which has been earlier demonstrated. However, a deviation from the numerical simulation is noticed due to the bistability of the system. Effectively, a quasiperfect coincidence is observed until $N = 6$, but beyond, the ring locks into the inner limit cycle so that the $K_{bn}(2)$ values should be calculated now with $A_0 = 0.343$, and probably around another resonance value $\delta = n^2$, n being an integer greater than 1.

The same comment can be made for the bifurcation from spatiotemporal chaos to instability. The intermediate double line stands for the semianalytical and analytical boundaries corresponding to the chaotic trajectory, and the single lower solid line stands for the bifurcation boundary related to the inner limit cycle. Once again, the numerical comparison rapidly switches from the chaotic boundary to the periodic one. Therefore, since in the $\gamma < 0$ case the spectral invariance condition is not fulfilled, several bifurcation boundary values do coexist. Consequently, depending on the number of oscillators and on the initial conditions, the ring's state variables will bifurcate around various boundary lines related to the different spectral groups.

IV. CONCLUSION

In this paper we have studied the various dynamical states of a shift-invariant set of diffusely coupled single-well Duffing oscillators. A general stability analysis has led to an uncoupled set of canonical Mathieu equations, and Floquet theory has been used with effect to derive analytical stability boundaries for the spatial Fourier modes of the model. We have also analyzed the Hopf transitions from spatiotemporal chaos to cluster and complete synchronization states through the Strutt diagram. At last, a scaling law has enabled us to deduce the stability pattern of any N ring from the two-oscillators model Lyapunov spectrum.

This study can be extended to other models of coupled oscillators, provided that they have a relatively strong fundamental Fourier component, as is the case for Rössler-like oscillators [4,6,9]. It would also be of great interest to develop the statistical approach of the model in the thermodynamic limit, and also to extend the analytical study to the related continuous medium model. At last, more precise physical and biological models sometime require us to consider nonlocal couplings [5] or long-range interactions [7]. For these latter cases, interesting new phenomena have yet been observed through numerical simulations, and are waiting for accurate analytical explanations.

[1] K. S. Fink, G. Johnson, T. Carroll, D. Mar, and L. Pecora, Phys. Rev. E **61**, 5080 (2000).

[2] M. Zhan, G. Hu, and J. Yang, Phys. Rev. E **62**, 2963 (2000).

[3] G. Hu, J. Xiao, J. Gao, X. Li, Y. Yao, and H. Bambi, Phys. Rev. E **62**, R3043 (2000).

[4] Y. Zhang, G. Hu, H. A. Cerdeira, S. Chen, T. Braun, and Y. Yao, Phys. Rev. E **63**, 026211 (2001).

[5] V. N. Belykh, I. V. Belykh, and E. Mosekilde, Phys. Rev. E **63**, 036216 (2001).

[6] Y. Zhang, G. Hu, and H. A. Cerdeira, Phys. Rev. E **64**, 037203 (2001).

[7] S. E. de S. Pinto, S. R. Lopes, and R. L. Viana, Physica A **303**, 339 (2002).

[8] D. K. Umberger, C. Grebogi, E. Ott, and B. Afeyan, Phys. Rev. A **39**, 4835 (1989).

[9] J. F. Heagy, T. L. Carroll, and L. M. Pecora, Phys. Rev. E **50**, 1874 (1994); Phys. Rev. Lett. **74**, 4185 (1995).

[10] H. G. Winful and L. Rahman, Phys. Rev. Lett. **65**, 1575 (1990); G. V. Osipov, A. S. Pikovsky, M. C. Rosenblum, and J. Kurths, Phys. Rev. E **55**, 2353 (1997).

[11] U. Parlitz and W. Lauterborn, Phys. Lett. A **107**, 351 (1985); C. Pezeschki and E. H. Dowell, Physica D **32**, 194 (1988); A. H.-D. Cheng, C. Y. Yang, K. Hackl, and M. J. Chajes, Int. J. Non-Linear Mech. **28**, 549 (1993); J. L. Summers, J. Brindley, P. H. Gaskell, and M. D. Savage, Philos. Trans. R. Soc. London, Ser. A **354**, 143 (1996).

[12] P. Woafo and R. A. Kraenkel, Phys. Rev. E **65**, 036225 (2002).

[13] Y. Chembo Kouomou and P. Woafo, Phys. Lett. A **298**, 18 (2002).

[14] N. J. Corron, Phys. Rev. E **63**, 055203 (2001).

[15] Y. Chembo Kouomou and P. Woafo, Phys. Rev. E **66**, 036205 (2002).

[16] Y. Chembo Kouomou and P. Woafo, Phys. Rev. E **66**, 066201 (2002).